A Unified Design for ZVT PWM Converters With Resonant Auxiliary Circuit

M. L. Martins, J. Russi, H. A. Gründling, H. Pinheiro, J. R. Pinheiro and H. L. Hey

Power Electronics and Control Research Group - GEPOC
Federal University of Santa Maria - UFSM
97105-900 - Santa Maria - RS – Brazil
mariolsm@terra.com.br, jumar.russi@bol.com.br, hey@ctlab.ufsm.br - www.ufsm.br/gepoc

Abstract – **The Zero-Voltage Transition (ZVT) PWM Converters with Resonant Auxiliary Circuit (RAC) are gathered and analyzed by means of a common topology derived in the paper. Its operation modes are identified and analyzed. A novel state-plane approach is proposed to determine the soft-switching conditions boundary to this sort of ZVT PWM converters. Moreover, a unified design criterion, based on the analytical definition of the soft-switching boundary, is described in details. By means of the proposed criterion, the time spent with repetitive numerical simulation of a given topology to define its design guidelines based on some set of particular features can be quite reduced.**

The theoretical analysis is confirmed by means of experimental results obtained from a ZVT PWM boost converter, which operates at 1 kW, 100 kHz.

I. INTRODUCTION

With the progress that electronics has been experienced in the last years, small size and weight equipments have become a requirement of today industry. To accomplish these features an increase in converters switching frequency is almost unavoidable. Nevertheless, at high switching frequency levels, switching losses become of prime concern. To alleviate the trade-off between converter power and switching frequency, soft-switching techniques have been often employed.

Among the soft-switching techniques, the ZVT has been used [1-10]. This technique employs a low power-rated auxiliary circuit in parallel with the main power path, so enabling the converter to work closely as possible to its PWM counterpart, with low conduction losses compared to other zero voltage switching techniques [11].

To control the power flow between the low power-rated auxiliary and main power circuit, some elements are required.

In this paper a special group of ZVT converters is investigated. These converters make use of a resonant tank to accomplish power flow control. The sinusoidal shape of the voltage and current through the auxiliary circuit, resulting from the resonant tank operation, leads to a simple way to control the converter power direction between main and auxiliary circuits.

However, one inconvenient presented by this group of converters is a third order resonant process that occurs during main switch turn-on process, which makes inappropriate the utilization of the well-known state-plane analysis as a simple geometric tool, as presented in [12,13]. In addition, the auxiliary circuit main parameters, as well as characteristic impedances and resonant frequencies cannot be directly calculated. In these cases, converter parameters are, usually, determined by graphs or characteristic curves, which show how variables such as components stresses and soft-switching boundaries vary in function of circuit parameters, [4,5,8,10]. These curves are obtained by means of several numerical simulations of the converter circuit requiring large computational efforts. Furthermore, to obtain useful graphs from the computed data, some parameters must be kept at constant values. This fact can reduce the range of validity of the analysis. A consequence derived from this situation is a rambling set of design guidelines that cannot be used to draw any conclusion about the features of a particular topology despite others.

In this paper is proposed a novel geometrical approach which allows the analytical determination of the ZVS conditions for the ZVT converters with Resonant Auxiliary Circuit (ZVT-RAC), i. e., for third order ZVT converters. As the analytical soft-switching conditions boundary is determined it can be used to derive a unified design guidelines. In addition, by means of this design guidelines, main converter features can be easily derived.

This paper is organized as follows: Section II introduces the ZVT PWM converters with RAC and describes the operation modes that can be assumed by them. Section III presents a linear transformation that permits a two-dimension representation of their three variable state-planes. In Section IV the soft-switching conditions are derived by means of the state-planes defined in previous Section. In Section V The ellipsis approach is introduced and thoroughly described and analyzed. Section VI presents a illustrative design guideline and example. In Section VII the analysis is proved by means of experimental results obtained from a ZVT PWM boost laboratory prototype rated at 1 kW operating at 100 kHz. Finally, Section VIII presents the conclusions from the analysis and the experimental results. In the appendix is shown the validation of the elliptical method.

II. ZVT PWM CONVERTERS WITH RAC

In DC-DC PWM converters, switching process is accomplished by an active/passive switch pair, which forms a single-pole double-throw switch (SPDT), which is commonly referred as PWM switch [14]. To minimize the ripple caused by the PWM switch action, low-pass filter elements are added to the SPDT. In its simplest form the SPDT with low-pass indutive filter can be used as a unified circuit, named *common DC-DC converter cell* – CCC, to represent any of the DC-DC PWM converters, Fig. 1(a), [15]. Assuming that the current through the inductors is almost constant in a switching cycle, the circuit can be simplified as depicted in Fig. 1(b). Disregarding the current source I_1 and the capacitance C_{s2}, ZVS can be performed for one switching direction by utilizing current I to charge the snubber capacitor C_{S1} placed in parallel with switch S. On the other hand, in the opposite switching direction it is necessary to utilize the auxiliary circuit to redirect the inductor current I before to charge the snubber capacitor C_{S1}, Fig 1(c). In addition, after main switch be in on state, current through auxiliary circuit must be completely diverted back to main power path. To

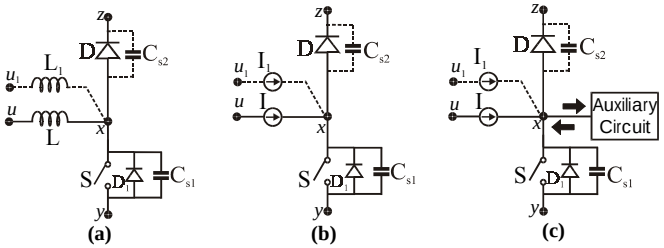

Fig. 1 –PWM converter circuit diagrams. (a) Basic PWM cell; (b) Simplified PWM cell; (c) PWM switching cell and auxiliary circuit.

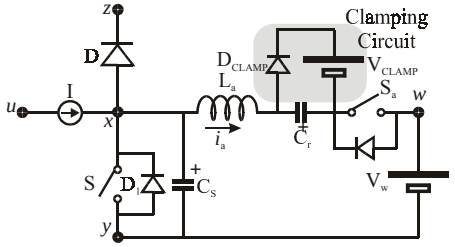

Fig. 2 – Basic ZVT PWM converter diagram with clamping.

accomplish current direction control some auxiliary element(s) must play(s) the role of a voltage source, which will directly control the voltage polarity across the auxiliary inductor L_r. In the ZVT-RAC converters analysed in this paper, a resonant capacitor, C_r, plays this role.

To obtain a unified analysis for ZVT-RAC during main switch turn-on process [4-10], a basic topology is shown in Fig. 2. Despite the following analysis being carried out for a boost ZVT converter it can be applied to other DC-DC non-isolated converter topologies, as the *common DC-DC converter cell* is reported.

A.Operation Analysis of ZVT-RAC

The basic topology consists of: a snubber capacitor (C_s), resonant inductor (L_r) and capacitor (C_r), a current bi-directional switch (S_a) and a clamping circuit comprised by a clamping diode and a clamping voltage source, V_{Clamp}. Since the terminal *w* could be connected to any of the CCC terminals, *y*, *z* and *u*, a generic DC voltage source, V_w, can be used to represent these different connections.

In steady state during turn-on process of switch S, the circuit of Fig. 2 can operate in three different operation modes: (i) the mode where the clamping voltage is not reached and the clamping diode never conducts, referred as Operation Mode 1 - OM_1; (ii) the mode where the clamping voltage is reached before the capacitor C_s to be completely discharged, referred as Operation Mode 2 - OM_2; and, (iii) the mode where the clamping voltage is reached after the capacitor C_s to be completely discharged, referred as Operation Mode 3 - OM_3.

Depending on the operation mode, the converter can assume six or seven circuit stages in a switching period, Fig 3.

The circuit stages are described as follow. Before S_a to be turned-on, both switches are off and diode D conducts current I. When S_a is turned on (Stage 1), the inductor current i_{Lr} starts to increase in a resonant way until it reaches I. With diode D blocked, (Stage 2) the capacitor C_s joins the resonant process until v_{Cs} falls to zero (OM_1, OM_3) or v_{Cr} reaches V_{Clamp} (OM_2). During Stage 3a (OM_1, OM_3), body-diode D_1 keeps v_{Cs} clamped at zero. Thus, ZVS was ensured for switch S. i_{Lr} and v_{Cr} keep resonating until i_{Lr} reaches I (OM_1) or v_{Cr} clamps (OM_3). For Stage 3b (OM_2) diode D_{Clamp} is in on state and v_{Cr} is clamped to V_{Clamp}. v_{Cs} drops in a resonant way until it reaches zero. In Stage 4 (OM_2, OM_3) v_{Cs} is clamped to zero by D_1 and i_{Lr} decreases at a constant gradient $(V_W+V_{Clamp})/L_r$. During Stage 5a (OM_1) current is transferred from the auxiliary circuit to S in a resonant fashion until i_{Lr} to be equal to zero. For Stage 5b (OM_2, OM_3) the resonant process is over and the current through S increases linearly until i_{Lr} falls to zero. In Stage 6, due to the positive charge stored in C_r, body-diode D_{Sa} keeps conducting and i_{Lr} goes negative. This mode ends when i_{Lr} returns to zero.

It can be seen that the three operation modes comprises different circuit stages: OM_1 is formed by stages S0, S1, S2, S3a, S5a, S6 and S7; Likewise, OM_2 consist of stages S0, S1, S2, S3b, S4, S5b, S6 and S7; and OM_3 is comprised by stages S0, S1, S2, S3a, S4, S5b, S6 and S7. The relationship among these different operation modes is shown by the flowchart of Fig. 4.

III. State-Plane Analysis

The differential equations, which define the state-plane for the three operation modes (depicted in Fig. 3) of the converter are described in this section. To obtain only circular arcs and straight lines in the state-plane trajectories a appropriate transformation is applied on its state variables.

Stage 1: Applying the Kircchoff Voltage Law (KVL) to the circuit, the differential equations which represent the variable behavior in the first resonant stage are,

$$\begin{cases} \dot{i}_{Lr}(t)=\left[V_{Cs}(t)-V_{Cr}(t)-V_w\right]/L_r \\ \dot{v}_{Cs}(t)=0 \\ \dot{v}_{Cr}(t)=\left[i_{Lr}(t)\right]/C_r \end{cases} \quad (1)$$

These equations, which represent a 3rd order system are difficult to solve by the conventional time domain approach. Nevertheless,

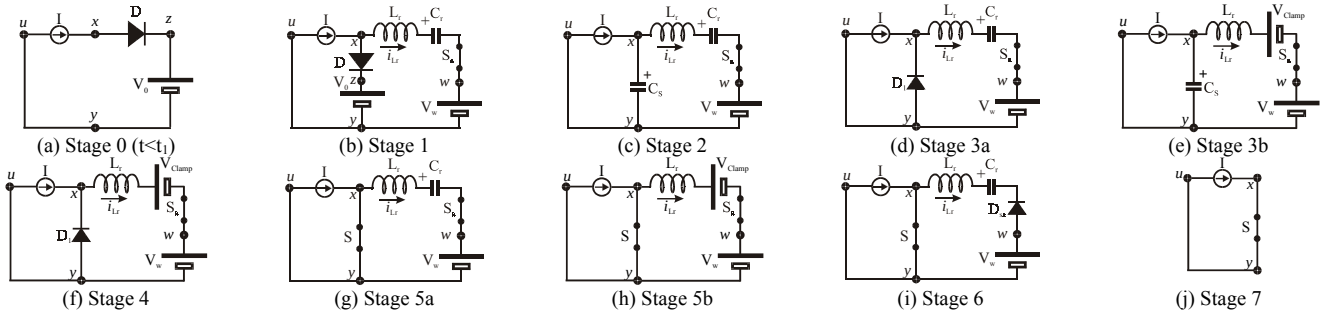

Fig. 3 – Diagram of the circuit modes of common ZVT-RAC.

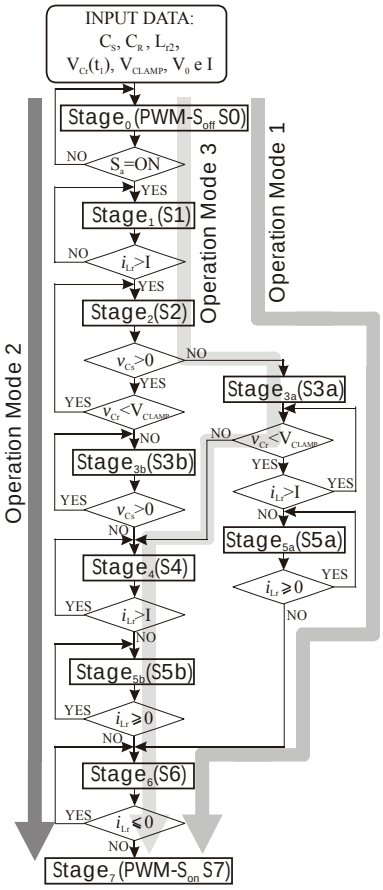

Fig. 4 – Converter Operation Flowchart.

by a proper transformation on its state variables, the steady state solution of (1) can be derived from a two-dimensional state-plane diagram. Defining a new state variable $v_C(t)$ as a linear combination of $v_{Cs}(t)$ and $v_{Cr}(t)$ as,

$$v_C(t)=v_{Cs}(t)-v_{Cr}(t), \tag{2}$$

the differential equation given by (1) can be simplified as follows,

$$\begin{cases} \dot{v}_C(t)=-\left[i_{Lr}(t)\right]/C_r \\ \dot{i}_{Lr}(t)=\left[v_C(t)-V_w\right]/L_r \end{cases} \tag{3}$$

Normalizing (3) by Z_rI and I, it can be written as

$$\begin{cases} \dot{v}_{C\_n}(t)=-\omega_r\left[i_{Lr\_n}(t)\right] \\ \dot{i}_{Lr\_n}(t)=\omega_r\left[v_{C\_n}(t)-V_{w\_n}\right] \end{cases} \tag{4}$$

where

$$Z_r=\sqrt{L_r/C_r}\ ;\ \ \omega_r=1/\sqrt{L_rC_r} \tag{5}$$

And $v_{C\_n}=v_C/(Z_rI)$, $i_{Lr\_n}=i_{Lr}/I$, $V_{w\_n}=V_w/(Z_rI)$.

In terms of the state equation form, (4) can be written as

$$\frac{dv_{C\_n}(t)}{di_{Lr\_n}(t)}=\frac{-\omega_r\left[i_{Lr}(t)\right]}{\omega_r\left[v_{C\_n}(t)-V_{w\_n}\right]} \tag{6}$$

Solving expression (6) one can find,

$$\left(v_{C\_n}(t)-V_{w\_n}\right)^2+\left(i_{Lr\_n}(t)-0\right)^2=\left(v_{C\_n}(t_{S1})-V_{w\_n}\right)^2 \tag{7}$$

Stage 2: The second resonant stage differential equations are,

$$\begin{cases} \dot{i}_{Lr}(t)=\left[v_{Cs}(t)-v_{Cr}(t)-V_w\right]/L_r \\ \dot{v}_{Cs}(t)=\left[I-i_{Lr}(t)\right]/C_s \\ \dot{v}_{Cr}(t)=\left[i_{Lr}(t)\right]/C_r \end{cases} \tag{8}$$

Using the state variable $v_C(t)$ defined by (2) and the normalization factors ZI and I, the state equation is as follows,

$$\frac{dv_{C\_n}(t)}{di_{Lr\_n}(t)}=\frac{\omega\left[\left(1-(\omega_r/\omega)^2\right)-i_{Lr\_n}(t)\right]}{\omega\left[v_{C\_n}(t)-V_{w\_n}\right]}. \tag{9}$$

Where

$$Z=\sqrt{L_r/C_{eq}}\ ;\ \ \omega=1/\sqrt{L_rC_{eq}};\ C_{eq}=C_rC_s/(C_r+C_s) \tag{10}$$

Solving expression (9) one can find,

$$\left(v_{C\_n}(t)-V_{w\_n}\right)^2+\left(i_{Lr\_n}(t)-\left(1-(\omega_r/\omega)^2\right)\right)^2 =\left(v_{C\_n}(t_{S2})-V_{w\_n}\right)^2+(\omega_r/\omega)^4 \tag{11}$$

Stages 3a, 5a and 6: The resonant stages 3a, 5a and 6 can be by,

$$\begin{cases} \dot{i}_{Lr}(t)=\left[v_{Cs}(t)-v_{Cr}(t)-V_w\right]/L_r \\ \dot{v}_{Cs}(t)=0 \\ \dot{v}_{Cr}(t)=\left[i_{Lr}(t)\right]/C_r \end{cases} \tag{12}$$

By $v_C(t)$ and the normalization factors Z_rI and I, the state equation form can be written for this stage as follows,

$$\frac{dv_{C\_n}(t)}{di_{Lr\_n}(t)}=\frac{-\omega_r\left[i_{Lr\_n}(t)\right]}{\omega_r\left[v_{C\_n}(t)-V_{w\_n}\right]} \tag{13}$$

Solving expression (13) one can find,

$$\left(v_{C\_n}(t)-V_{w\_n}\right)^2+\left(i_{Lr\_n}(t)-0\right)^2=\left(v_{C\_n}(t_{Si})-V_{w\_n}\right)^2+\left(i_{Lr\_n}(t_{Si})\right)^2 \tag{14}$$

Where $t_{Si}=t_{S3a}$ for Stage 3a, $t_{Si}=t_{S5a}$ for Stage 5a nd $t_{Si}=t_{S6}$ for Stage 6.

Stage 3b: The resonant stage 3b is represented by,

$$\begin{cases} \dot{i}_{Lr}(t)=\left[V_{Cs}(t)-V_{Cr}(t)-V_w\right]/L_r \\ \dot{v}_{Cs}(t)=\left[I-i_{Lr}(t)\right]/C_s \\ \dot{v}_{Cr}(t)=0 \end{cases} \tag{15}$$

By $v_C(t)$ and normalization factors Z_sI and I, from (15),

$$\frac{dv_{C\_n}(t)}{di_{Lr\_n}(t)}=\frac{\omega_s\left[1-i_{Lr\_n}(t)\right]}{\omega_s\left[v_{C\_n}(t)-V_{w\_n}\right]} \tag{16}$$

where

$$Z_s=\sqrt{L_r/C_s}\ ;\ \ \omega_s=1/\sqrt{L_rC_s} \tag{17}$$

Solving expression (16) one can find,

$$\left(v_{C\_n}(t)-V_{w\_n}\right)^2+\left(i_{Lr\_n}(t)-1\right)^2=\left(v_{C\_n}(t_3)-V_{w\_n}\right)^2+\left(i_{Lr\_n}(t_{S3b})-1\right)^2 \tag{18}$$

Stage 4 and 5b: The stages 4 and 5b are represented by,

$$\begin{cases} \dot{i}_{Lr}(t)=\left[V_{CLAMP}+V_w\right]/L_r \\ \dot{v}_{Cs}(t)=\dot{v}_{Cr}(t)=0 \end{cases} \tag{19}$$

By $v_C(t)$ and normalization factors ZI and I, (19) becomes,

$$i_{Lr\_n}(t)=I_{Lr\_n}(t_{Si})-\omega_i\left(V_{Clamp\_n}+V_{w\_n}\right)t \tag{20}$$

Where $\omega_i=\omega_s$ for OM_2, $\omega_i=\omega_r$ for OM_3, $t_{Si}=t_{S4}$ for Stage 4 and $t_{Si}=t_{S5b}$ for Stage 5b;

Stages 0 and 7: The stages 0 and 7 are governed by the PWM modulation and represent a dead point in the state-plane trajectory.

The state-plane trajectories for OM_1, OM_2 and OM_3, are drawn, respectively, from the following expressions: (7), (11) and (14); (7), (11), (20) and (14); (7), (11), (14), (20) and (14), Fig. 5. Due to the different normalized variables (depending on each circuit mode), a same actual inductor current, $i_{Lr}(t)$, would result in different normalized variables. Thus, discontinuities in the state-plane trajectory may occur in the circuit mode boundaries.

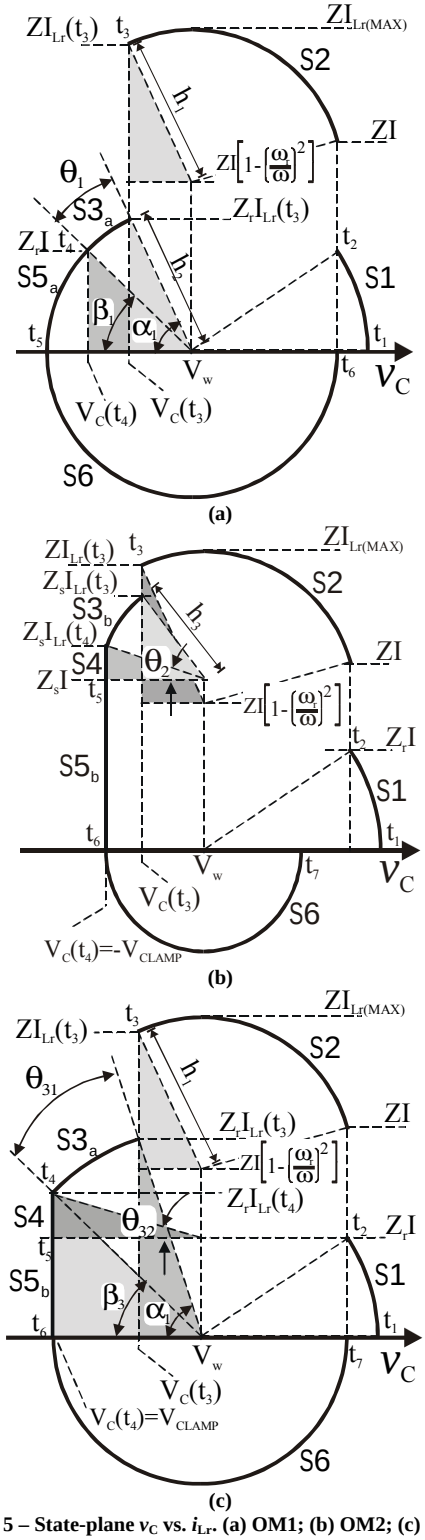

Fig. 5 – State-plane v_C vs. i_{Lr}. (a) OM1; (b) OM2; (c) OM3.

IV. Soft-Switching Conditions

A. Operation Mode 1

To ensure soft-switching conditions for S, at instant t_3, its body-diode must be turned on. By state-plane depicted in Fig. 5(a), in OM_1, it can be seen that the following expression must be ensured,

$$\theta_1 = \alpha_1 - \beta_1 \geq 0 \tag{21}$$

where α_1 and β_1 are defined from the highlighted triangles by the expressions below,

$$\alpha_1 = \mathrm{tg}^{-1}\left(I_{Lr}(t_3)Z_r / \left(V_w - V_C(t_3)\right)\right) \tag{22}$$

$$\beta_1 = \sin^{-1}\left(IZ_r / h_2\right) \tag{23}$$

The constant h_2 is common for both triangles and can be defined by the Pythagorean theorem as follows,

$$h_2 = \sqrt{\left(V_w - V_C(t_3)\right)^2 + \left(Z_r I_{Lr}(t_3)\right)^2} \tag{24}$$

Therefore, expression (21) can be written as,

$$\theta_1 = \mathrm{tg}^{-1}\left(\frac{I_{Lr}(t_3)Z_r}{V_w - V_C(t_3)}\right) - \sin^{-1}\left(\frac{IZ_r}{\sqrt{\left(V_w - V_C(t_3)\right)^2 + \left(I_{Lr}(t_3)Z_r\right)^2}}\right) \tag{25}$$

It can be seen that θ_1 is a function of converter parameters such as, V_w, Z_r and I; and the voltage and current through resonant elements at instant t_3.

B. Operation Mode 2

In the OM_2, to ensure soft-switching conditions for S, at t_3 its body-diode must be turned on. By the state-plane depicted in Fig. 5(b), it can be seen that,

$$\theta_2 = \cos^{-1}\left(\left(V_w - V_C(t_4)\right)/h_3\right) \geq 0 \tag{26}$$

Where, $V_C(t_4) = -V_{CLAMP}$ and the constant h_3 is obtained from the highlighted triangle, as follows,

$$h_3 = \sqrt{\left(V_w - V_C(t_3)\right)^2 + \left(Z_s\left(I_{Lr}(t_3) - I\right)\right)^2} \tag{27}$$

Thus, expression (26) can be written as,

$$\theta_2 = \cos^{-1}\left(\frac{V_W + V_{CLAMP}}{\sqrt{\left(V_w - V_C(t_3)\right)^2 + \left(Z_s\left(I_{Lr}(t_3) - I\right)\right)^2}}\right) \tag{28}$$

It can be seen that θ_2 is a function of converter parameters such as, V_{CLAMP}, V_w, Z_s and I; and the voltage and current through resonant elements at instant t_3.

C. Operation Mode 3

In the OM_3, to assure that main switch will be turned on under soft-switching conditions, at t_3 its body diode must be turned on. By the state-plane depicted in Fig. 5(c), it can be seen that this condition is ensured by the following expression

$$\theta_3 = \theta_{31} + \theta_{32} \geq 0 \tag{29}$$

where,

$$\theta_{31} = \alpha_1 - \beta_3, \text{ and} \tag{30}$$

$$\theta_{32} = tg^{-1}\left(Z_r\left(I_{Lr}(t_4)-I\right)/\left(V_C(t_4)+V_W\right)\right). \quad (31)$$

By trigonometric identities one can obtain,

$$\beta_3=\cos^{-1}\left(\left(V_W\text{-}V_C(t_4)\right)/h_4\right). \quad (32)$$

As $V_C(t_4) = -V_{CLAMP}$, it is necessary to define $I_{Lr}(t_4)$. Thus,

$$h_4=\sqrt{\left(V_w\text{-}V_C(t_4)\right)^2+\left(I_{Lr}(t_4)Z_r\right)^2} \quad (33)$$

or

$$h_4=\sqrt{\left(V_w\text{-}V_C(t_3)\right)^2+\left(I_{Lr}(t_3)Z_r\right)^2} \quad (34)$$

From (33) and (34), $I_{Lr}(t_4)$ can be defined as,

$$I_{Lr}(t_4)=\sqrt{\left(V_w\text{-}V_C(t_3)\right)^2+\left(I_{Lr}(t_3)Z_r\right)^2-\left(V_w+V_{CLAMP}\right)^2}\Big/Z_r \quad (35)$$

Therefore, expression (29) can be written as follows,

$$\theta_3 = \text{tg}^{-1}\left(I_{Lr}(t_3)Z_r/\left(V_w\text{-}V_C(t_3)\right)\right)-\cos^{-1}\left(\left(V_{CLAMP}+V_W\right)/h_4\right) + tg^{-1}\left(Z_r\left(I_{Lr}(t_4)-I\right)/\left(V_{CLAMP}+V_W\right)\right) \quad (36)$$

It can be seen that θ_3 is a function of converter parameters such as, V_{CLAMP}, V_w, Z_s and I; and the voltage and current through resonant elements at instant t_3.

As one can see, the soft-switching conditions angles θ_1, θ_2 and θ_3 are dependent of the state-plane point ($V_C(t_3)$, $I_{Lr}(t_3)$). Thus it is required to develop the expression to define this point to assure the converter operation under soft-switching conditions.

D. Definition of Voltage V_C (t_3)

Using trigonometric identities in the common triangle for the three state-planes of Fig. 4., $V_C(t_3)$ can be defined as,

$$V_C(t_3)=V_w+Z\sqrt{\left(I_{Lr(MAX)}\text{-}I\left(\omega_s/\omega\right)^2\right)^2-\left(I_{Lr}(t_3)\text{-}I\left(\omega_s/\omega\right)^2\right)^2} \quad (37)$$

Where $I_{Lr(max)}$ is the maximum value achieved by the current through resonant inductor and can be given by,

$$I_{Lr(MAX)}=I\left(\omega_s/\omega\right)^2+\sqrt{I\left(\omega_r/\omega\right)^2+\left(\left(V_w+V_C(t_2)-V_o\right)/Z\right)^2} \quad (38)$$

And also,

$$V_C(t_2)=V_o\text{-}V_w\text{-}\left(V_o\text{-}V_w\text{-}V_C(t_1)\right).\sqrt{1-\left(\frac{I.\omega_r.L_r}{V_o\text{-}V_w\text{-}V_C(t_1)}\right)^2} \quad (39)$$

It can be seen that $V_C(t_3)$ is a function of converter parameters such as, ω_r, ω_s, ω, Z, V_w, $V_C(t_1)$; and of current, $I_{Lr}(t_3)$. Therefore, the angles that define soft-switching conditions for the three operation modes θ_1 , θ_2 and θ_3 are still a function of $I_{Lr}(t_3)$.

V. ELLIPSIS APPROACH

Considering that the information required to ensure that current $I_{Lr}(t_3)$ is greater than I when voltage v_{Cs} reaches (or is very close to) zero at instant t_3, is lost during the singularity transformation applied to the state variables, it is necessary to draw another state-plane trajectory than that of Section III. As v_{Cs} is the variable of interest, the state-plane $v_{Cs}(t)$ vs. $i_{Lr}(t)$ becomes the focus of the analysis. This state-plane trajectory is characterized by having a 3rd order resonant process resulting in an oval arc. A close observation of this state-plane segment reveals that it is very close to an elliptical arc, or a stretched circular arc. Such effect is caused by the linear charge of the parallel equivalent capacitors C_s and C_r by input current source I, as it can be seen by expression (40).

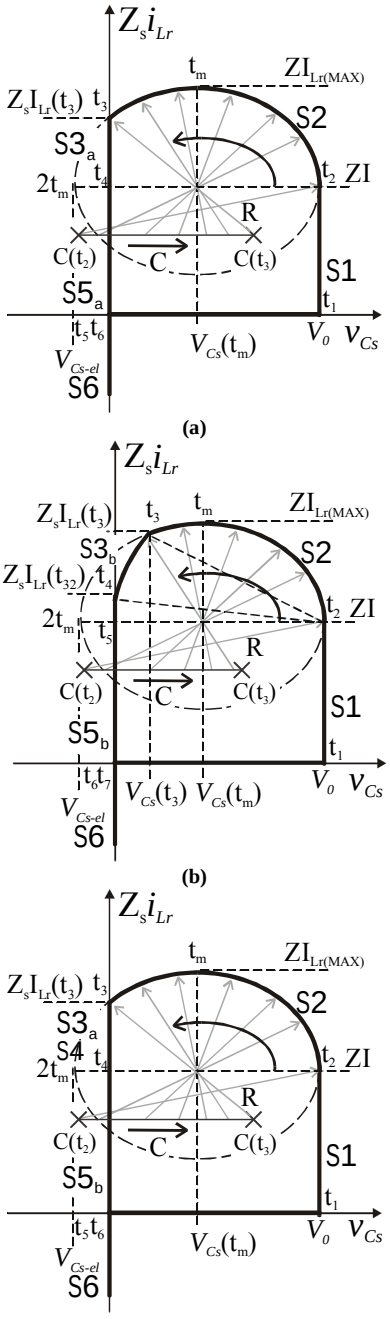

Fig. 6 - State-plane v_{Cs} vs. i_{Lr}. (a) OM1; (b) OM2; (c) OM3.

$$v_{Cs(LIN-CHR)}=It/\left(C_s+C_r\right) \quad (40)$$

The linear charge defined by (40) moves the center of the resonant process to the right, represented by the straight line "C" with initial conditions at point $C(t_2)$ and final conditions at point $C(t_3)$, Fig 6. The verification of the ellipsis theorem is demonstrated in the Appendix.

The expression that describes the ellipsis is,

$$\left(\left(2V_{Cs}(t)\text{-}V_{Cs\text{-}el}\text{-}V_0\right)/\left(V_0\text{-}V_{Cs\text{-}el}\right)\right)^2+\left(\left(I_{Lr}(t)\text{-}I\right)/\left(I_{Lr(max)}\text{-}I\right)\right)^2=1 \quad (41)$$

Where $V_{Cs\text{-}el}$ is the minimum voltage that $V_{Cs}(t)$ would obtain without being clamped by the body diode of S and it is given by

$$V_{Cs\text{-}el}=V_1\cos(2\omega t_m)+V_2\sin(2\omega t_m)+V_3 \quad (42)$$

where

$$t_m=tg^{-1}(-V_1/V_2)/\omega \quad (43)$$

$$V_1=(\omega_s/\omega)^2(V_0-V_{Cr}(t_2)-V_w), \quad (44)$$

$$V_2=((\omega_r/\omega)Z_r-Z)(\omega_r/\omega)^2 I, \quad (45)$$

$$V_3=V_w+V_{Cr}(t_2)+(I2t_m/(C_r+C_s))+(\omega_r/\omega_{eq})^2(V_0-V_{Cr}(t_2)-V_w). \quad (46)$$

A. Operation Mode 1

In the OM1 at instant t_3, capacitor C_s is completely discharged, $V_{Cs}(t_3)=0$. Therefore, from (41), $I_{Lr}(t_3)$ can be found as,

$$I_{Lr}(t_3)=I+(I_{Lr(max)}-I)\sqrt{-4V_{Cs\text{-}el}V_0/(V_0-V_{Cs\text{-}el})^2} \quad (47)$$

Thus, substituting (37) and (47) into (25), it can be seen that,

$$\theta_1=f\{I,V_0,V_{Cr}(t_1),C_s,C_r,L_r\}\geq 0. \quad (48)$$

And, hence, as I and V_0 are defined by the converter load specifications, the remaining parameters, $V_{Cr}(t_1)$, that represents the initial conditions of capacitor C_r, and the auxiliary elements C_s, C_r and L_r can be chosen by the designer to ensure the soft-switching conditions.

B. Operation Mode 2

In the OM2 at instant t_3, C_s is not completely discharged. Therefore, by expression (41), $I_{Lr}(t_3)$ can be found as a function of $V_{Cs}(t_3)$. Substituting (37) into (41), $I_{Lr}(t_3)$ is given as follows,

$$I_{Lr}(t_3)=I+(I_{Lr(max)}-I)\sqrt{1-\left[\frac{2(V_{Cs}(t_3)-V_{CLAMP})-V_{Cs\text{-}el}-V_0}{V_0-V_{Cs\text{-}el}}\right]^2} \quad (48)$$

This way, substituting (37) and (48) into (28), it can be seen that,

$$\theta_2=f\{I,V_0,V_{CLAMP},V_{Cr}(t_1),C_s,C_r,L_r\}\geq 0. \quad (49)$$

As I and V_0 are defined by the converter load specifications, the remaining parameters $V_{Cr}(t_1)$, that represents the initial voltage of the capacitor C_r, V_{Clamp} and the elements C_s, C_r and L_r are defined by the designer of the auxiliary circuit and hence, they can be chosen to ensure the soft-switching conditions.

C. Operation Mode 3

Likewise the OM1, at instant t_3, C_s is completely discharged. Hence, $I_{Lr}(t_3)$ is given by expression (47). Substituting (37) and (47) into (36), it can be seen that,

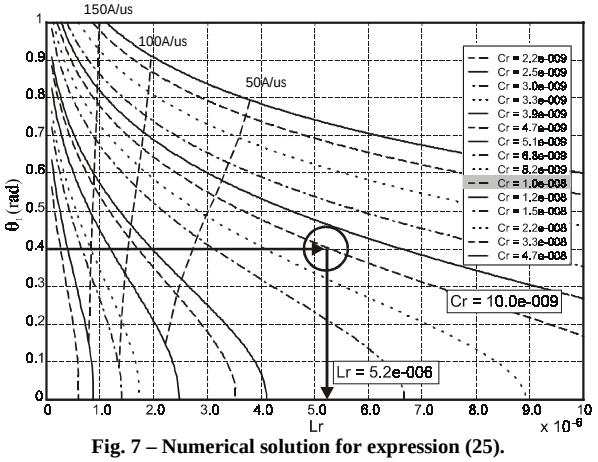

Fig. 7 – Numerical solution for expression (25).

TABLE 1–TOPOLOGY PARAMETERS

Reference	V_w	V_{Clamp}	$V_{Cr}(t_1)$
[4]	V_0	Zero	$-2V_0$
[5]	Zero	-----	$f\{L_r, C_s, C_r, R_{Damp}\}$
[6,7]	Zero	-----	Zero
[8]	Zero	-----	$f\{N, L_r, C_s, C_r, C_{r2}\}$
[9]	Zero	V_0	$-V_0$
[10]	Zero	-----	$f\{L_r, C_s, C_r, C_{r2}\}$

$$\theta_3=f\{I,V_0,V_{CLAMP},V_{Cr}(t_1),C_s,C_r,L_r\}\geq 0. \quad (50)$$

Therefore, the parameter V_{Clamp} and elements C_s, C_r and L_r can be defined by the designer to ensure the soft-switching conditions.

VI. DESIGN GUIDELINES AND EXAMPLES

Since the expressions that define the soft-switching conditions for the ZVT-RAC, for each operation mode, were obtained, they can be used in practical examples. With this purpose a ZVT PWM boost converters will be designed by means of the analytical definition of its soft-switching conditions.

For this example, the ZVT converter presented in [6,7], which operates according to OM_1, was chosen to be designed with the new design guidelines. In this example the converter specification are as follows. The converter circuit delivered 1kW (2.5A/400V) to a resistive load, at a 100 kHz switching frequency, and is supplied by a $150V_{DC}$ voltage source. The auxiliary circuit components are defined below as follows.

1. Step 1: C_s is defined as a turn-off capacitive snubber by the following expression [16],

$$C_s=It_f/\sqrt{12}V_0=687\,pF. \quad (51)$$

Where t_f is equal 136ns (t_f+$t_{D(OFF)}$ of IRFP450). As the MOSFET output capacitance (C_{oss}) varies non-linearly as function of drain to source voltage and its effective value is about two or three times smaller than the presented by the data sheet (C_{oss}= 720pF, V_{DS}= 25V) [17], a 1nF discrete capacitor was chosen to implement C_s.

2. Step 2: The choice of the converter topology also defines the following parameters V_w, V_{Clamp} and $V_{Cr}(t_1)$, as shown in Table 1. For [6,7] the parameters are V_w=0V, V_{Clamp}=-V_0, $V_{Cr}(t_1)$=0V. Once C_s and the topology parameters are well defined, L_r and C_r can be found for a given value of the angle θ_1 by means of expression (25). As the algebraic solution of (25) is not trivial, it is solved numerically and the results are depicted in the abacus of Fig. 7. To aid the choice of the auxiliary elements, the abacus is divided in ranges of boost diode *di/dt*, which is defined by the expression below,

$$di/dt=\sqrt{(V_o-V_w-V_C(t_2))^2-(IZ_r)^2}/L_r. \quad (52)$$

Defining θ_1 equal to 0.4. and a capacitance (C_r) of 10 nano-Farads, the resulting inductance (L_r) is approximately 5.0 micro-Henry, as can be seen in Fig. 6. The on time of the body-diode of S

TABLE 2–EXPERIMENTAL SPECIFICATIONS AND PARAMETERS

Component	Parameters	Device	Parameters
V_i	150 V_{DC}	S	IRFP450
P_0 (f_s)	1 kW (100kHz)	D	MUR1560
L	0.91 mH	S_a	HGTP3N60C3D
C	150 uF	D_{Clamp}	RHRP8120
L_r	5.2µH		
C_s	1nF		
C_r	10.0nF		

is calculated by the following expression

$$\Delta t_{on} = \theta_1 / \omega_r = \theta_1 \sqrt{L_r C_r} \approx 93ns \cdot \quad (53)$$

VII. Experimental Results

To evaluate the theoretical analysis, the ZVT converter designed in the previous Section, a laboratory prototype has been implemented. The converter power stage is shown in Fig. 8.

The prototype parameters are described in Table 2.

In Fig. 9 the experimental results are shown. Fig. 9 (a) shows the waveforms for the main switch. It can be seen that main switch turn-on occurs under ZVS conditions. Fig. 9(b) shows that the voltage across C_r never reaches the clamping voltage, characterizing the operation in mode 1 of the topology. The main switch commutation waveforms can be seen in detail in Fig. 9(c), which reveals that the measured conduction time of main switch body-diode (about 90ns) is very close to the value previously calculated (93 ns).

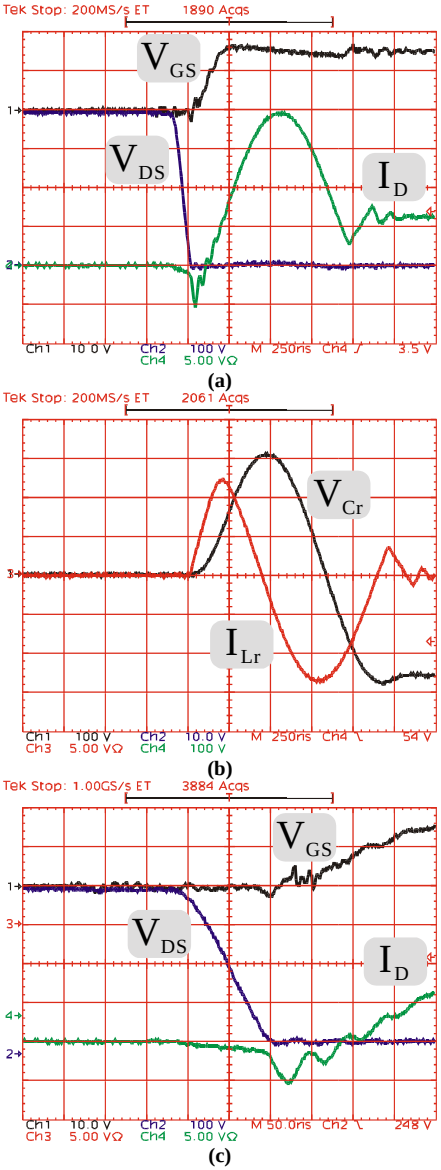

Fig. 9 – Commutation experimental waveforms. (a) Main switch; (b) Resonant Circuit; (c) Main switch, detail.

VIII. Conclusions

This paper presented a complete state-plane analysis for ZVT PWM Converters with an auxiliary resonant circuit (ZVT-RAC), which are characterized by a third order state-space variable. Due to its complexity and lack of information, the ZVT-RAC state-plane analysis is usually avoided and replaced by other graphical analyses.

To overcome the lack of information presented by third order state-space variable analyses presented to date, this paper presented a novel state-plane analysis. The proposed analysis obtains the remaining information necessary to ensure the converter soft-switching conditions from an auxiliary elliptical state-plane. Therefore, the soft-switching conditions can be obtained directly from the geometrical relations of the converter state-planes.

Moreover, to obtain a generalized methodology to derive the ZVT-RAC state-planes and related soft-switching conditions, all the analysis is carried out by means of a common ZVT circuit. The operation modes, governing equations and state-planes for this common ZVT circuit, were presented, as well as a operation mode flowchart.

In addition, a unifying design methodology is presented to simplify the design process of ZVT-RAC converters. Likewise other sort of ZVT converters (with second order auxiliary resonant circuits), this methodology is based on the soft-switching boundary.

The theoretical analysis is verified by experimental results obtained from a ZVT PWM boost converter, operating at 1kW, 100 kHz, which confirmed the calculated results.

References

[1] Hua, G., Leu, C.-S., Lee, F. C., "Novel Zero-Voltage-Transition PWM Converters", in *IEEE Power Electronics Specialists Conference*, p. 55-60, 1992;

[2] Gegner, J.P., Lee, C.Q., "Zero-Voltage-Transition Converters Using an Inductor Feedback Technique", *in IEEE Applied Power Electronics Conference*, Vol.2, p. 862-868, Ninth Annual, 1994;

[3] Filho, N. P., Farias, V. J., Freitas, L. C., "A Novel Family of DC-DC PWM Converters Using the Self-Resonance Principle", *in IEEE Power Electronics Specialists Conference*, p. 1385-1391, 1994;

[4] Yang, L., Lee, C. Q., "Analysis and Design of Boost Zero-Voltage-Transition PWM Converter", in *IEEE Applied Power Electronics Conference*, p. 707-713,

[5] Moschopoulos, G., Jain, P., Joos, G., "A Novel Zero-Voltage Switched PWM Boost Converter", in *IEEE Power Electronics Specialists Conference*, p. 694-700, 1995;

[6] Smith, K. M., Smedley, K. M., "A Comparison of Voltage-Mode Soft-Switching methods for PWM Converters", in *IEEE Transactions on Power Electronics*, Vol. 12, n. 2, p. 376-386, 1997;

[7] Tseng, C.-J., Chen, C.-L., "Novel ZVT-PWM Converters With Active Snubbers", in *IEEE Transactions on Power Electronics*, Vol. 13, n. 5, p. 861-869, 1998;

[8] Moschopoulos, G., Jain, P., Joos, G., "A Zero-Voltage Switched PWM Boost Converter With An Energy Feedforward Auxiliary Circuit", in *IEEE Power Electronics Specialists Conference*, p. 076-082, 1996;

[9] D. M. Xu, J. M. Zhang, Y. C. Ren, Z. Qian, "A Novel Single-Phase Active-Clamped ZVT-PWM PFC Converter", *in IEEE Applied Power Electronics Conference*, p. 456-459, 2000;

[10] Jain, N., Jain, P., Joos, G., "Analysis of a Zero-Voltage Transition Boost Converter Using a Soft Switching Auxiliary Circuit with Reduced Conduction Loss", in *IEEE Power Electronics Specialists Conference*, Vol. 4, p. 1799-1804, 2001;

[11] Hua, G., Leu, C.-S., Lee, F. C., "Soft-Switching Techniques in PWM Converters", in *IEEE Trans. On Industrial Electronics*, Vol. 42, Issue 6, p. 595-603, 1995;

[12] Oruganti, R., Lee, F. C. "Resonant Power Processors, Part I- State-Plane Analysis" in *IEEE Trans. On Industry Applications* Vol. IA-21, Issue 6,

pp. 1453-1460, 1985;
[13] Oruganti, R., Lee, F. C. "State-Plane Analysis of Parallel Resonant Converter" in *IEEE Power Electronics Specialist Conference*, pp. 56-73, 1985;
[14] Tymerski, R., Vorpérian, V., Lee, F. C., Baumann, W. T., "Nonlinear Modeling of the PWM Switch" in *IEEE Trans. on Power Electronics*, Vol. 4, Issue 2, p. 595-603, 1999.
[15] Stein, C. M. O.; Hey, H.L.;, **"**A New Family of Soft-Switching DC-DC PWM Converters Using a True ZCZVT Commutation Cell", in *IEEE IECON 98*, p. 1030 –1035;
[16] P. T. Krein, *Elements of Power Electronics.* New York and Oxford: Oxford University Press, 1998;
[17] "A More Realistic Characterization Of Power MOSFET Output Capacitance Coss", International Rectifiers Application note, AN-1001.

APPENDIX

A. Correlation between converter state-plane trajectory and an ellipsis.

An elliptical curve can be defined by the following expression

$$\left((x-x_0)/a\right)^2+\left((y-y_0)/b\right)^2=1. \tag{54}$$

where,

x, y – associated variables;

x_0, y_0 – geometrical center;

a – distance from the center to vertical top;

b – distance from the center to horizontal edge;

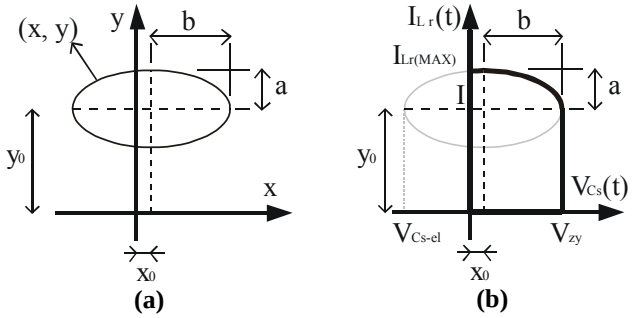

Fig. 10 – Elliptical State Plane (a) Ellipsis; (b) V_{Cs}(t) vs I_{Lr}(t).

The following equations relate the state plane V_{Cs}(t), I_{Lr}(t) with the ellipsis:

$$b=\left(V_{zy}+V_{Cs-el}\right)/2, \tag{55}$$

$$a=I_{Lr(MAX)}-I, \tag{56}$$

$$x=V_{Cs}(t), \tag{57}$$

$$y=I_{Lr}(t). \tag{58}$$

$$x_0=\left(V_{Cs-el}+V_{zy}\right)/2. \tag{58}$$

$$y_0=I. \tag{58}$$

where,

V_{zy} – voltage V_0 in the case of a boost converter;

V_{Cs-el} – Minimum voltage value for V_{Cs}(t) (disregarding main switch body diode).

Substituting a, b, x and y from (55), (56), (57) and (58) into (54), it can be found

$$\left(\frac{V_{Cs}(t)-\left(V_{zy}+V_{Cs-el}\right)/2}{V_{zy}-\left(V_{zy}+V_{Cs-el}\right)/2}\right)^2+\left(\frac{I_{Lr}(t)-I}{I_{Lr(MAX)}-I}\right)^2=1 \tag{59}$$

Rewriting it

$$\left(\frac{2V_{Cs}(t)\text{-}V_{Cs-el}\text{-}V_{zy}}{V_{zy}\text{-}V_{Cs-el}}\right)^2+\left(\frac{I_{Lr}(t)\text{-}I}{I_{Lr(MAX)}\text{-}I}\right)^2=1 \tag{60}$$

B. Procedure Validation

To evaluate the error generated when the state-plane trajectory is approximated by an ellipsis the eccentricity was calculated according to:

a) Substituting (55), (56) in expression (61)

$$\varepsilon=\sqrt{a^2-b^2}/a \tag{61}$$

The eccentricity can be calculated for a given ellipsis by

$$\varepsilon_c=\sqrt{\left(I_{Lr(MAX)}-I\right)^2-\left(\left(V_{zy}+V_{Cs-el}\right)/2\right)^2}\Big/\left(I_{Lr(MAX)}-I\right) \tag{62}$$

b) From the ellipsis definition (54) it can be obtained

$$a=\left(x-x_0\right)b\Big/\sqrt{b^2-\left(y-y_0\right)^2} \tag{63}$$

Substituting (63) in (61)

$$\varepsilon_{sp}=\frac{\sqrt{\left(\left(V_{Cs}(t)-x_0\right)b\right)^2-\left(b^2-\left(I_{Lr}(t)-I\right)^2\right)b^2}}{\left(V_{Cs}(t)-x_0\right)b} \tag{64}$$

It can be seen that expression (62) is defined only by constant circuit parameters, while expression (64) is defined by state-plane variables. Subtracting expressions (64) from (62) an error function is obtained between the theoretical ellipsis (62) and the ellipsis formed by the state-plane variables.

Fig. 11 shows the error calculated for the design of Section V evaluated for 2,000 points.

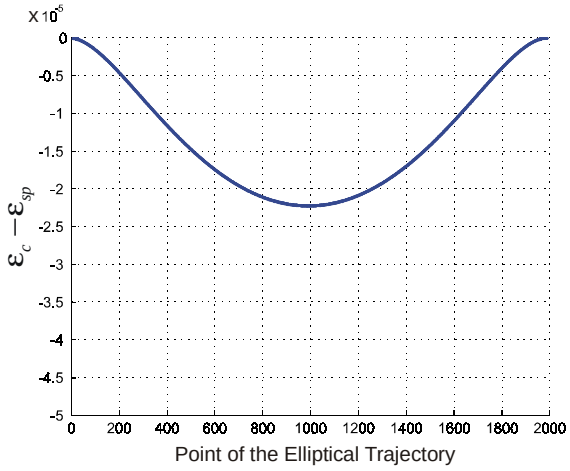

Fig. 11. Calculated Error.